Structure and Chemical Bonding in Zr-Doped Anatase TiO_2 Nanocrystals

P. E. Lippens,*,† A. V. Chadwick,‡ A. Weibel,§ R. Bouchet,§ and P. Knauth§

Institut Charles Gerhardt, AIME, CNRS UMR 5253, CC015, Université Montpellier II, F-34095 Montpellier Cedex 05, France, School of Physical Sciences, University of Kent, Canterbury, Kent CT2 7NH, United Kingdom, and MADIREL, Université de Provence-CNRS (UMR 6121), Centre St Jérôme, F-13397 Marseille Cedex 20, France

Received: July 26, 2007

Zirconium-doped anatase TiO_2 nanopowders and nanoceramics with particle sizes between 12 and 30 nm were investigated by EXAFS spectroscopy. Furthermore, ab initio calculations based on density functional theory were performed to analyze changes in the electronic structure due to Zr doping. Zr is dissolved on substitutional bulk sites with a slight increase of the bond lengths of the inner coordination shells. The Debye−Waller factors show that the nanocrystallites are highly ordered. There is no indication for defect states or band gap changes with Zr doping.

1. Introduction

Defects in general and interfaces in particular (e.g., grain boundaries in ceramics and phase boundaries in composites) strongly impact the properties of materials.[1,2] Size reduction of solids leads to the domain of nanostructured materials, which is currently a hot topic in research and development.[3] Advanced nanosized materials have recently attracted considerable interest in the domain of Li-ion batteries because electrochemical properties are very sensitive to particle size and connectivity.

Another strategy for improving properties is doping. However, the success of this operation depends on the site where the dopant ion is placed: dopant ions will impact the properties in a different way if they are placed substitutionally on regular bulk sites, on interstitial positions, or segregated to boundaries. Extended X-ray absorption fine structure (EXAFS) spectroscopy is an element-specific technique sensitive to short-range order, which provides information on the local structure around a target ion. It is ideally suited to locating the sites occupied by dopants.[4]

Anatase phase titanium dioxide is nowadays studied for many applications in the energy and environment sector, including photocatalysis,[5] photovoltaic energy conversion and photoelectrochemical cells,[6] reducing gas sensors,[7] and lithium battery anodes.[8] We have previously reported EXAFS studies of different dopants in anatase TiO_2: an acceptor, Zn, a donor, Nb,[9] and an isovalent cation, Sn.[10] EXAFS showed that Sn and Nb are essentially dissolved on substitutional bulk sites, whereas Zn is mainly segregated in space charge regions near surfaces and grain boundaries.

In this work, we extended our previous approach to zirconium, a dopant that is four-valent, like titanium, and has a slightly larger cation radius. Calculations based on density functional theory (DFT) were performed to analyze the changes in the bond length and electronic structure of TiO_2 due to Zr doping. The bond lengths can be compared to experimental data obtained from EXAFS. From a fundamental point of view, the conjunction of EXAFS spectroscopy and ab initio calculations is a unique tool to study the local environment around a zirconium ion in terms of bond lengths and electronic structure and to obtain a very complete picture of the bonding around Zr ions at low concentrations.

2. Experimental Procedures

2.1. Sample Preparation. Pure anatase nanopowders were obtained by precipitation from sulfuric acid solutions by heating to 95−110 °C (sulfate route).[11] For zirconium doping, the corresponding amount of $Zr(CH_3COO)_4$ was added before precipitation. The precipitates were thoroughly washed and calcined for 1 h at 300 or 600 °C.

Nanocrystalline anatase ceramics were prepared by hot-pressing nanopowders calcined at 600 °C under 0.45 GPa in pure alumina dies. The powders were heated by a 5 K/min up to the final temperature, where they remained for 2 h. The final temperature was adjusted to the average size of the powder particles: for the powders calcined at 600 °C, 580 °C is sufficient to reach more than 90% relative density ceramics. The pressure was then released, and the ceramic was cooled with an intrinsic cooling rate of the hot-press (Cyberstar). The density of the nanocrystalline ceramics was determined from mass and geometrical dimensions and confirmed by dilatometric experiments and mercury porosimetry. Densities of 92 ± 1% of theory, based on the density of pure anatase, were obtained under these conditions.

The mean grain size and size distribution of the nanopowders and nanoceramics were studied by transmission electron microscopy (TEM), BET adsorption measurements, and X-ray diffraction (XRD). We have recently compared the most usual techniques for the determination of average grain size and grain size distribution, specifically for the case of nanocrystalline materials.[12]

2.2. EXAFS. The EXAFS experiments were performed at station X1 of the Hamburg Synchrotron facility (Hasylab, DESY Hamburg). The synchrotron has a positron energy of 4.45 GeV, and the average current during the measurements was 100 mA. Fluorescence Zr K-edge spectra were recorded at room temperature. The nanoceramic sample was used as-pressed (6 mm diameter × 1 mm thickness). The doped powder samples were

* Corresponding author. E-mail: lippens@univ-montp2.fr.
† Institut Charles Gerhardt.
‡ University of Kent.
§ Université de Provence.

10.1021/jp075898u CCC: $40.75
Published on Web 12/13/2007

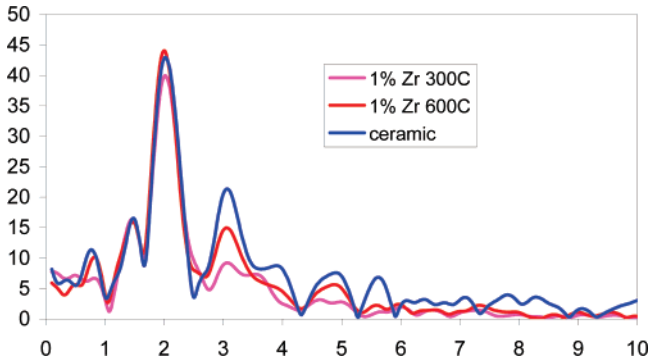

Figure 1. Fourier transformed Zr K-edge EXAFS spectra for 1 mol % Zr-doped TiO_2 powder calcined at 300 and 600 °C and 1 mol % doped TiO_2 nanocrystalline ceramic, corrected with the phase shift of the first shell. The best fit parameters for the EXAFS data are given in Table 1 for seven-shell fitting and in Table 2 for four-shell fitting.

TABLE 1: Zr K-Edge Data, Seven-Shell Fitting

	EXAFS 1% 600 °C			EXAFS 1% 300 °C			EXAFS ceramic		
atom	CN	RD (Å)	A (Å^2)	CN	RD (Å)	A (Å^2)	CN	RD (Å)	A (Å^2)
O	6	2.047	0.013	6	2.053	0.015	6	2.047	0.012
Ti	4	3.098	0.022	4	3.111	0.032	4	3.096	0.019
Ti	4	3.902	0.016	4	3.906	0.014	4	3.889	0.019
O	8	4.069	0.013	8	4.024	0.010	8	4.098	0.029
O	16	4.468	0.084	16	4.220	0.030	16	4.113	0.048
O	4	4.618	0.005	4	4.548	0.016	4	4.631	0.003
Ti	8	4.846	0.024	8	4.797	0.030	8	4.848	0.022
	E_o = 7.50 eV; R = 33.4%			E_o = 7.88 eV; R = 36.2%			E_o = 7.4 9 eV; R = 33.0 %		

prepared by being pressed into pellets with polyethylene as the binder. EXAFS data analysis was performed with EXCALIB, EXBACK, and EXCURV98 computer programs developed at the Daresbury synchrotron.[13] Phase shifts were derived from ab initio calculations within EXCURV98. This code also includes routines to treat multiple scattering effects in highly symmetric structures. For each spectrum, a theoretical fit was obtained by adding shells of atoms around the central excited atom and least-squares iterating the edge position, E_0, radial distances, RD, and the Debye−Waller type factors, A. This latter factor contains contributions from both thermal disorder and static variations in RD. The coordination number, CN, can also be iterated. The quality of the fit is measured by an R-factor, and the errors in RD are about 0.02 Å in A and about 20% in CN.

3. Theory

The atomic positions of Zr-doped TiO_2 were obtained by DFT calculations[14] from the CASTEP code and the pseudo-potential plane-wave formalism.[15] The generalized gradient approximation (GGA) with the exchange-correlation potential by Perdew et al.[16] and ultrasoft pseudo-potentials[17] were used for the calculations. Two different supercells of 48 atoms: $ZrTi_{15}O_{32}$ (2 × 2 × 2) and 108 atoms: $ZrTi_{35}O_{72}$ (3 × 3 × 2), respectively, were considered to test the finite size effects and possible interactions between the Zr atoms. In the two cases, the plane-wave kinetic energy cutoff was set to 400 eV. The k-space sampling was performed on a Monkhorst-Pack grid with 9 and 1 k-points in the irreducible Brillouin zone for the 48 atom and 108 atom supercells, respectively. All atom positions were relaxed within the supercells, but the lattice parameters were kept fixed at the experimental values of anatase TiO_2: a = 3.78 Å and c = 9.51 Å.[18] The mechanical equilibrium was achieved through conjugate gradient minimization of the total energy to a tolerance of 10^{-5} eV, the forces to a tolerance of 0.03 eV Å^{-1}, and the atomic positions to a tolerance of 10^{-3} Å. A density mixing scheme with a conjugate gradient Pulay solver was used for the energy minimization, and a BFGS algorithm was used for the internal coordinate optimization. The electronic structure was evaluated from a more accurate all-electron calculation based on DFT-GGA with the same exchange-correlation potential and the atomic positions obtained from the pseudo-potential calculation for the 48 atom supercell. We have made use of the full-potential linearized augmented plane-wave method (FLAPW) as implemented in the WIEN code.[19] With this method, the unit cell is partitioned into atomic spheres centered at the atomic positions and an interstitial region. The muffin-tin radii were r_{mt}(Ti) = 2.0 au, r_{mt}(O) = 1.4 au, and r_{mt}(Zr) = 2.2 au. To improve the energy linearization, the basis set was extended with Ti 3s, Ti 3p, O 2s, Zr 4s, and Zr 4p local orbitals. In the interstitial region, the wave functions were expanded in plane waves with wavenumbers K such as min(r_{mt})max(K) = 7, and the charge density was expanded in a Fourier series with G_{max} = 15 Ry$^{-1/2}$. The irreducible wedge of the Brillouin zone was sampled using 30 points.

4. Results and Discussion

Figure 1 shows a comparison of Fourier transformed Zr K-edge EXAFS spectra of nanocrystalline 1 mol % Zr-doped anatase TiO_2 powder calcined at 300 and 600 °C with a nanocrystalline anatase ceramic. The EXAFS spectra are very similar showing consistently the Zr−O and Zr−Ti coordination shells. One can conclude that the dopant sits on substitutional Ti positions. The corresponding bond distances and Debye−Waller factors are reported in Table 1 with seven-shell fitting and in Table 2 using four-shell fitting.

The bond distances calculated from EXAFS for 1% Zr doping reported in Tables 1 and 2 are consistently about 0.1 Å larger than in pure anatase for the two first coordination shells and similar for outer shells. This corresponds to the slightly higher radius of the octahedrally coordinated tetravalent zirconium cation (r(Zr^{4+}) = 0.72 Å) in comparison to the host titanium cation (r(Ti^{4+}) = 0.60 Å).[20] The Debye−Waller factors are small, even below those obtained for Ti K-edge, and consistent

TABLE 2: Zr K-Edge Data, Four-Shell Fitting

	EXAFS 1% 600 °C			EXAFS 1% 300 °C			EXAFS ceramic		
atom	CN	RD	A (Å^2)	CN	RD	A (Å^2)	CN	RD	A (Å^2)
O	6	2.050	0.013	6	2.066	0.015	6	2.049	0.013
Ti	4	3.099	0.021	4	3.118	0.031	4	3.098	0.014
Ti	4	3.898	0.017	4	3.927	0.019	4	3.871	0.013
O	8	4.072	0.017	8	4.093	0.015	8	4.061	0.015
	$E_o = 7.04$ eV; $R = 34.7$ %			$E_o = 7.31$ eV; $R = 37.8$%			$E_o = 8.34$ eV; $R = 52.7$%		

TABLE 3: Values of Zr−O and Zr−Ti Bond Lengths (Å) for the Seven First Coordination Shells Given[a]

	theory: unrelaxed	theory: relaxed	exptl
Zr−O	4 × 1.93	4 × 2.02 (2.01)	6 × 2.05
	2 × 1.99	2 × 2.11 (2.11)	
Zr−Ti	4 × 3.03	4 × 3.10 (3.11)	4 × 3.10
Zr−Ti	4 × 3.78	4 × 3.81 (3.79)	4 × 3.89
Zr−O	8 × 3.84	8 × 3.86 (3.86)	8 × 4.10
Zr−O	8 × 4.24	8 × 4.25 (4.25)	16 × 4.11
	8 × 4.28	8 × 4.31 (4.31)	
Zr−O	4 × 4.77	4 × 4.80 (4.80)	4 × 4.63
Zr−Ti	8 × 4.85	8 × 4.85 (4.85)	8 × 4.85

[a] Results are given for the unrelaxed and relaxed supercells of 108 atoms (theory) and from the EXAFS data of the ceramic samples (experimental). The theoretical bond lengths obtained for a supercell of 48 atoms are also given for comparison (in parentheses).

with the heavier Zr ions, highly ordered on substitutional sites inside the nanocrystallites.

The theoretical Zr−X (X = O or Ti) bond lengths are given in Table 3 for both the 48 atom and the 108 atom supercells. The values obtained for the two supercells are within 0.01 Å, which confirms the weak influence of the interactions between the Zr periodic images. The averaged relaxed Zr−X bonds are larger than unrelaxed bonds by about 0.1 and 0.06 Å within the first and second coordination shells, respectively, in excellent agreement with the results obtained from EXAFS. However, only calculations make possible the distinction between the two very close bond lengths in the first coordination shell. The local Zr environment formed by the two first coordination shells is similar to that of Ti in undoped TiO_2 (Figure 2). The first shell is formed by six O atoms. Two of them are along the *c*-axis (axial oxygen atoms: O_{ax}) and are distant from Zr by 2.11 Å (+0.11 Å/Ti−O_{ax} in undoped TiO_2), whereas the other four oxygen atoms (equatorial oxygen atoms: O_{eq}) are distant from Zr by 2.02 Å (+0.09 Å/Ti−O_{eq} in undoped TiO_2). The angles between the four Zr−O_{eq} bonds and the *c*-axis are equal to 77°, which is close to the value obtained for O_{ax}−Ti−O_{eq} in undoped TiO_2 (78.6°). The second shell is formed by 4 Ti atoms at 3.10 Å (+0.06 Å/Ti−Ti in undoped TiO_2). The relaxation of the other bonds involving Zr does not exceed 0.03 Å. As expected, the observed main trend in the relaxation around Zr is the decrease of the bond length variations with increasing interatomic distance, showing that substitution of Zr for Ti mainly changes the two first coordination shells. The experimental values of the bond lengths for the third to sixth coordination shells (3.8−4.8 Å) differ from the calculated ones by about 0.1−0.2 Å. This could be due to the difficulties to extract these bond lengths from the EXAFS data as shown previously for Sn-doped TiO_2.[10]

The calculated total DOS of Zr-doped TiO_2 for the 48 atom supercell is shown in Figure 3. The energy reference is taken at the Fermi level, which is at the top of the valence band. Because of the small contribution of the Zr atom due to the composition of the supercell ($ZrTi_{15}O_{32}$), the main structures of the total DOS come from Ti and O atoms. The DOS is similar to that found for undoped TiO_2, and the main bands are labeled in the same way as in ref 10. The valence band, between −5 and 0 eV (labeled B), is formed by O 2p states hybridized with Ti 3d states, and the two lower conduction bands (labeled C and D), between 2.5 and 7.5 eV, are composed primarily of empty Ti 3d states. The structures C and D can be interpreted as molecular triply degenerate t_{2g} and doubly degenerate e_g states, respectively, due to interactions between Ti 3d and O 2p orbitals within the TiO_6 octahedra. The fine structures within these two groups can be related to the distortion of the octahedra

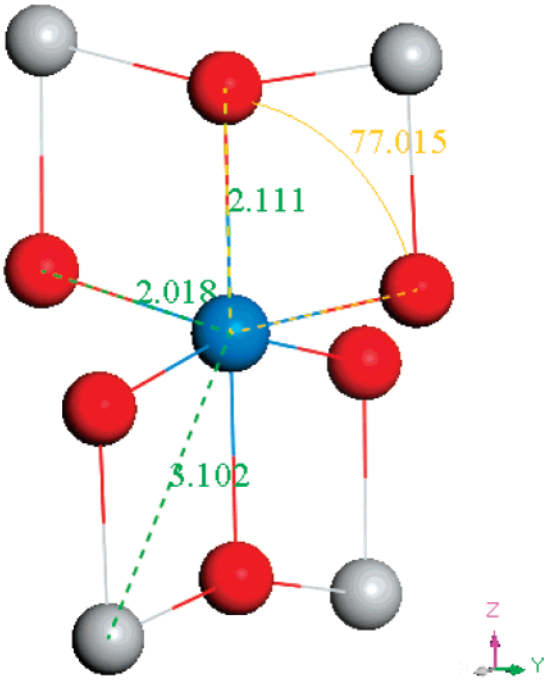

Figure 2. Local atomic structure of Zr (in blue) in Zr-doped TiO_2 as obtained from the pseudo-potential calculation for the 108 atom supercell. The first shell formed by oxygen atoms (in red) and the second shell formed by Ti atoms (in gray) are shown. The values of the bond lengths and angles are given in angstroms and degrees, respectively.

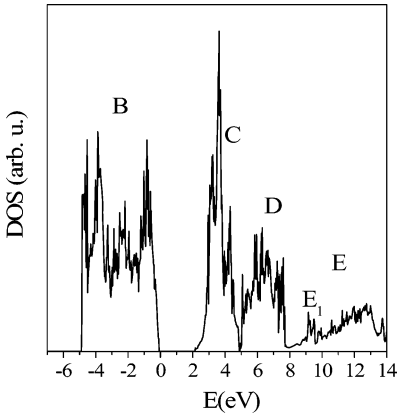

Figure 3. Calculated densities of states of Zr-doped TiO_2. The origin of the energy is taken at the Fermi level. The main features that are in common with undoped anatase TiO_2 are denoted by B−E, except for peak E_1, which is due to Zr.

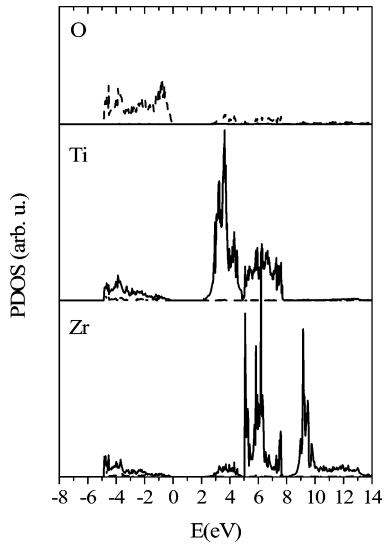

Figure 4. Calculated partial densities of states of Zr-doped TiO_2. The origin of the energy is taken at the Fermi level. The s (dotted line), p (dashed line), and d (solid line) states are averaged over the different crystallographic sites of each element of the supercell.

and to interactions with more distant atoms. The only significant difference is a small structure, at about 9.2 eV (labeled E_1), which occurs at the bottom of the band E mainly formed by delocalized empty states.

The partial DOS per atom are plotted in Figure 4. Except for small bond length variations, the Zr local environment is similar to that of Ti. As a result, interactions between Zr 4d and O 2p orbitals lead to bonding states within the valence band and antibonding states within the conduction bands that mainly contribute to the bands D and E_1 of the total DOS. Thus, the t_{2g} and e_g peaks of TiO_6 octahedra are found at about 4 and 6 eV, respectively, and those of the ZrO_6 octahedron at 6 and 9 eV, respectively. The energy shift of about 3 eV between these Ti and these Zr states can be related to the atomic energy difference between Ti 3d (−11 eV) and Zr 4d (−8.5 eV).[21] Of course, the contribution of Zr t_{2g} states to the peak D of the total DOS can be neglected as compared to the Ti e_g states, which is not the case for the Zr e_g states. This analysis shows that the substitution of Zr for Ti in TiO_2 anatase does not change noticeably the total DOS since the states are mainly found within the bands of TiO_2. It is of particular interest to note that the position of the Fermi level for the Zr-doped TiO_2 is unchanged as compared to undoped TiO_2 and that the band gap does not contain defect states. This clearly indicates that Zr doping of bulk TiO_2 does not improve the band gap dependent electronic properties, such as electronic conductivity or photocatalytic properties.

We have also evaluated the atomic charges to compare the ionic characters of the different bonds. The total charges found within the Zr and Ti muffin tin spheres by the LAPW calculation are about 3.0 and 2.5, respectively. Most of the Zr and Ti valence electrons have a d-type character, which is consistent with the partial DOS showing significant contributions in the valence band for the d-type states of these atoms. The observed difference between the charges indicates that Zr is more ionic than Ti, as expected from Pauling electronegativity differences: (O, 3.44; Ti, 1.54; and Zr, 1.33). A Mulliken population analysis was also performed with the CASTEP code for the 108 atom supercell. In this case, the Zr and Ti charges are 1.72 and 1.35, respectively. Although the values of the charges differ from those obtained from the LAPW calculation, as expected from their different definitions, they show the same trend, which is an increase of the cationic charge from Ti to Zr. The Mulliken charges on the O first neighbors of Zr are more negative (−0.73) than on the other O atoms of the supercell (−0.68). The overlap populations for $Zr-O_{eq}$ (0.33) and $Zr-O_{ax}$ (0.20) are lower than those of $Ti-O_{eq}$ (0.38) and $Ti-O_{ax}$ (0.23), respectively. This indicates that Ti−O bonds are more covalent than Zr−O bonds, which is consistent with the more ionic character of Zr as compared to Ti. An increase of the covalent character from the axial to the equatorial bonds is consistent with a decrease in the bond lengths. Thus, the substitution of Zr for Ti in TiO_2 provides more ionic Zr−O bonds as compared to Ti−O bonds by increasing the electron transfer toward the first O neighbors of Zr.

Finally, it is also interesting to compare the present results with our previous results obtained for Sn-doped TiO_2.[10] In the two cases, Sn^{4+} and Zr^{4+} are found to replace Ti^{4+} in the TiO_2 lattice with similar relaxation effects. First, there is no significant change in the local symmetry, and the distances with O first neighbors increase by about 0.1 Å, as expected from comparison between the ionic radii of the different tetravalent cations with octahedral coordination: $r(Ti^{4+}) = 0.60$ Å, $r(Sn^{4+}) = 0.69$ Å, and $r(Zr^{4+}) = 0.72$ Å.[20] Then, the interatomic distances increase in the two cases by about 0.06 Å with the Ti second neighbors and by less than 0.03 Å with the more distant neighbors. Finally, no improvements are expected in the electronic properties as compared to undoped TiO_2 since the position Fermi level and the band gap between the valence and the conduction bands are unchanged. However, the comparison between the local densities of states of Sn-doped TiO_2 (Figure 7 in ref10) and Zr-doped TiO_2 (Figure 4) clearly shows differences that are due to strong changes in chemical bonds involving hybridizations of O 2p states with Sn 5s and 5p states in one case and Zr 4d states in the other case.

5. Conclusion

Both EXAFS and DFT calculations show that the substitution of Zr^{4+} for Ti^{4+} in anatase TiO_2 leads to a slight increase of the bond lengths of the inner coordination shells. The density of states around the Fermi level does not change, and no defect levels occur in the band gap between the valence and the conduction bands.

Acknowledgment. Support from the European Union, in the framework of the ALISTORE network of excellence, and by the Agence Nationale de la Recherche ("LIBAN" project) is gratefully acknowledged.

Note Added after ASAP Publication. This article was released ASAP on December 13, 2007. Table 1 has been revised. The corrected version posted on December 21, 2007.

References and Notes

(1) Maier, J. *Prog. Solid State Chem.* **1995**, *23*, 171.
(2) Maier, J. *Physical Chemistry of Ionic Materials*; Wiley: Chichester, 2004.
(3) Edelstein, A. S.; Cammarata, R. C. *Nanomaterials: Synthesis, Properties, and Applications*; Institute of Physics Publishers: Bristol, 1996.
(4) Rush, G.; Chadwick, A. V. Characterization of Nanocrystalline Oxides by EXAFS Spectroscopy, in *Nanocrystalline Metals and Oxides*; Knauth, P., Schoonman, J., Eds.; Kluwer: Boston, 2002.
(5) Chang, S.; Dong, R. *J. Phys. Chem. B* **2006**, *110*, 20208.
(6) O'Regan, B.; Grätzel, M. *Nature (London, U.K.)* **1991**, *353*, 737.
(7) Carney, C. M.; Yoo, S.; Akbar, S. A. *Sensors Actuators, B* **2005**, *108*, 29.
(8) Huang, S. Y.; Kavan, L.; Exnar, I.; Grätzel, M. *J. Electrochem. Soc.* **1995**, *142*, 142.
(9) Bouchet, R.; Weibel, A.; Knauth, P.; Mountjoy, G.; Chadwick, A. V. *Chem. Mater.* **2003**, *15*, 4996.

(10) Weibel, A.; Bouchet, R.; Savin, S. L. P.; Chadwick, A. V.; Lippens, P. E.; Womes, M.; Knauth, P. *ChemPhysChem* **2006**, *7*, 2377.

(11) Knauth, P.; Bouchet, R.; Schäf, O.; Weibel, A.; Aeur, G. Functionalized TiO_2 Nanoparticles for Pigments, Photoelectro-Chemistry and Solid State Chemical Sensors, in *Synthesis, Functionalization, and Surface Treatments of Nanoparticles*; Baraton, M.-I., Ed.; American Science Publishers: Valencia, CA, 2002.

(12) Weibel, A.; Bouchet, R.; Boulc'h, F.; Knauth, P. *Chem. Mater.* **2005**, *17*, 2378.

(13) (a) Binsted, N.; Campbell, J. W.; Gurman, S. J.; Stephenson, P. C. *SERC Daresbury Program Library*; Daresbury Laboratory: Warrington, Cheshire, UK, 1992. (b) Binsted, N. *EXCURV98: CCLRC Daresbury Laboratory Computer Program*; Daresbury Laboratory: Warrington, Cheshire, UK, 1998.

(14) (a) Kohn, W.; Sham, L. J. *Phys. Rev. A: At., Mol., Opt. Phys.* **1965**, *140*, 1133. (b) Hohenberg, P.; Kohn, W. *Phys. Rev. B: Condens. Matter Mater. Phys.* **1964**, *136*, 864.

(15) Segall, M. D.; Lindan, P. L. D.; Probert, M. J.; Pickard, C. J.; Hasnip, P. J.; Clark, S. J.; Payne, M. C. *J. Phys.: Condens. Matter* **2002**, *14*, 2717.

(16) Perdew, J. P.; Burke, S.; Ernzerhof, M. *Phys. Rev. Lett.* **1996**, *77*, 3865.

(17) Vanderbilt, D. *Phys. Rev. B: Condens. Matter Mater. Phys.* **1990**, *42*, 7892.

(18) Horn, M.; Schwerdtfeger, C. F.; Meagher, E. P. *Z. Kristallogr.* **1972**, *136*, 273.

(19) Blaha, P.; Schwarz, K.; Luitz, J. *WIEN97*; Vienna University of Technology: Vienna, 1997 (improved and updated Unix version of the original copywright WIEN code, which was published by Blaha, P.; Schwarz, K.; Sorantin, P.; Trickey, S. B. *Comput. Phys. Commun.* **1990**, 59, 399).

(20) Shannon, R. D. *Acta Crystallogr., Sect. A: Found. Crystallogr.* **1976**, *32*, 751.

(21) Harrison, W. A. *Electronic Structure and Properties of Solids*; W. H. Freeman: San Francisco, 1980.